ACSNANO

www.acsnano.org

ARTICLE

Bioinspired Nanozymes as Nanodecoys for Urinary Tract Infection Treatment

Yihong Zhang,[#] Wanling Liu,[#] Gen Wei, Quanyi Liu, Guoqiang Shao, Xiang Gu, Xiaomiao Cui, Zijun Zhou, Yuting Wang, Sheng Zhao, Faheem Muhammad, Sirong Li, Tong Li, Yan Du, and Hui Wei*

Cite This: https://doi.org/10.1021/acsnano.3c12783

Read Online

ACCESS | Metrics & More | Article Recommendations | Supporting Information

ABSTRACT: Urinary tract infections (UTIs), common bacterial infections in communities and medical facilities, are mainly mediated by FimH. The glycan sites of the uromodulin protein play a crucial role in protecting against UTIs by interacting with FimH. A bioinspired approach using glycan-FimH interactions may effectively reduce bacteria through an antiadhesive mechanism, thereby curbing bacterial resistance. However, typical antiadhesive therapy alone fails to address the excessive reactive oxygen species and inflammatory response during UTIs. To bridge this gap, antioxidant nanozymes with antiadhesive ability were developed as nanodecoys to counter bacteria and inflammation. Specifically, ultrasmall dextran-coated ceria (DEC) was engineered to address UTIs, with dextran blocking FimH adhesion and ceria exhibiting anti-inflammatory properties. DECs, metabolizable by the kidneys, reduced bacterial content in the urinary tract, mitigating inflammation and tissue damage. In murine models, DECs successfully treated acute UTIs, repeated infections, and catheter-related UTIs. This dual approach not only highlights the potential of nanozymes for UTIs but also suggests applicability to other FimH-induced infections in the lungs and bowels, marking a significant advancement in nanozyme-based clinical approaches.

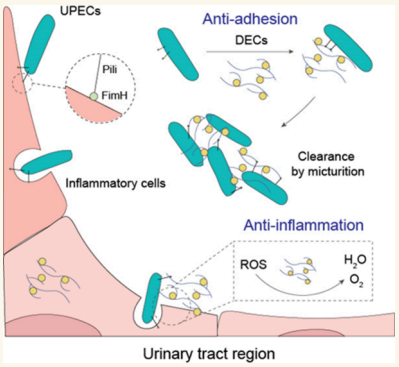

KEYWORDS: *anti-inflammation, antiadhesion, nanodecoy, nanozymes, reactive oxygen species, urinary tract infections*

INTRODUCTION

Urinary tract infections (UTIs) rank among the most prevalent bacterial infections, impacting millions of individuals and causing significant economic losses worldwide.[1,2] UTIs are primarily caused by uropathogenic *Escherichia coli* (UPEC). The pathogenic mechanism of UPEC-initiated UTIs involves bacterial adhesion, colonization, and the subsequent evasion of host immune responses.[3] The FimH adhesin within type 1 pili plays a crucial role in the invasion, adhesion, and persistence of UPECs by interacting specifically with mannosylated uroplakins and $\alpha_1\beta_3$ integrins on cell surfaces of the urinary tract.[4] This adhesion and colonization of pathogenic bacteria on the host cells determine the occurrence of diseases.

In response to bacterial invasions, some mammalian organisms have developed uromodulin (UMOD) to cope with external infectious threats.[5] The glycans within UMOD act as multivalent decoys, binding with FimH, inducing bacterial aggregation, and reducing cell invasion.[6] The bacteria with a weakened colonization ability are then expelled from the body through urine. Notably, a *UMOD* promoter variant drives a 2-fold increase in urinary UMOD concentration, resulting in reduced susceptibility to UTIs.[6] This innate defense mechanism relies mainly on interactions between FimH and UMOD's glycans. Therefore, creating a UMOD glycan-like binding site is a potential method for antiadhesive bacterial therapy. To date, a series of multivalent antagonists, designed as UMOD glycan mimetics and based on mannose and glucose structures, have been developed,[7−11] advancing clinical translation.[12,13] Although the multivalent strategy enhances the weak interaction between glycomimetics and FimH, the current glycomimetic-based antiadhesive therapeutics remain unsatisfactory due to their failure to address UPEC-induced inflammation.

When UTIs occur, the invasion by FimH[14] or other toxins, such as lipopolysaccharide (LPS),[15] triggers the release of inflammatory mediators, resulting in damage to the tissues colonized by bacteria, which in turn aggravates the infection.[2] Unfortunately, the use of antibiotics induces bacterial death, causing the release of bacterial contents and a more severe local inflammatory response.[16,17] Therefore, it is necessary to

Received: December 19, 2023
Revised: February 9, 2024
Accepted: February 13, 2024

develop therapeutics for regulating the inflammatory response during bacterial invasion, preventing adverse tissue damage, and halting disease progression.[18] Furthermore, since both UPEC bacteria and inflammation play critical roles in UTIs, the combination of antiadhesive and anti-inflammatory activities is a prudent strategy to treat UTIs.

Nanotechnology provides an effective implementation to integrate the antiadhesive and anti-inflammatory activities at the nanoscale. Among the emerging nanotechniques, nanozymes, the functional nanomaterials with enzyme mimicking activities, have shown promise in biomedicine due to their easy synthesis, low cost, and ease of modification.[19−22] The latter feature facilitates the incorporation of functionalities beyond catalysis, enabling biomimicry. In particular, antioxidant nanozymes have been developed to treat inflammatory diseases.[23−26] Among them, CeO_2 nanozyme has been extensively explored in various biomedical applications due to its superior biocompatibility and excellent anti-inflammatory activities.[27] Additionally, the engineerable surface of CeO_2 makes it facile for modifications. Therefore, we hypothesized that it is feasible to design a nanodecoy for UTIs therapy by endowing anti-inflammatory CeO_2 nanozyme with antiadhesive activity. To achieve this, we chose dextran (DEX) as the antiadhesive component for modifications. DEX, an FDA-approved biocompatible glycan composed of glucose molecules linked together in a branched fashion, offers multivalent sites for promising antiadhesive therapy.[28−30]

Herein, we report a bioinspired DEX-modified ceria (DEC) as a nanodecoy for UTI treatment. DEX enhanced the dispersion of ultrasmall ceria and, more importantly, provided multivalent binding sites for interacting with the FimH protein, thus simulating the functionality of UMOD and offering a platform for antiadhesive therapy (Scheme 1a). DECs showed superior antioxidant abilities in two types of cell lines toward oxidant stress driven by H_2O_2, LPS, and FimH. DECs effectively inhibited bacterial adhesion to cells and the abiotic surface. Significantly, the DECs demonstrated curative outcomes in the acute UTI model, repeated infection model, and catheter-associated UTI (CAUTI) model, highlighting their potential in future clinical applications (Scheme 1b).

Scheme 1. (a) Bioinspired Approach for Guiding the Synthesis of Carbohydrate-Based Nanodecoys (i.e., DECs) to Mimic UMOD (PDB: 7Q3N); (b) Renal Clearable Nanodecoys Possessing Antioxidant and Antiadhesive Abilities for the Treatment of UTIs

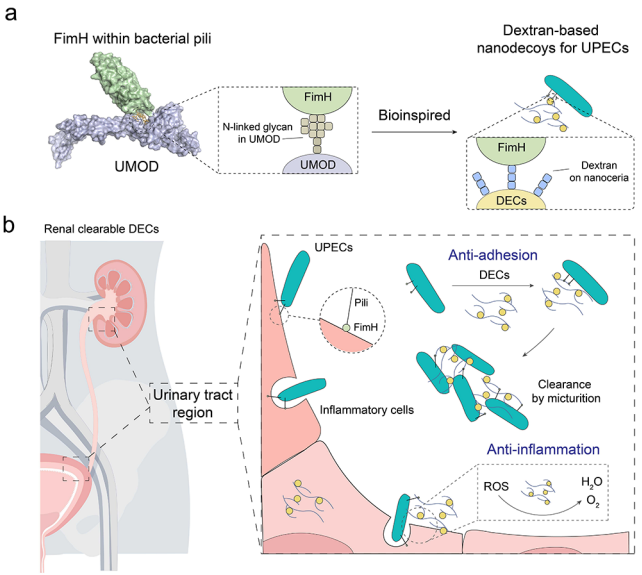

RESULTS AND DISCUSSION

Screening, Optimization, and Characterization of Nanodecoys. To highlight the importance of saccharides in nanodecoy design, we chose citric acid (CA), polyvinylpyrrolidone (PVP), and DEX as modifications to decorate the nanoceria. As shown in Figure 1a, the X-ray diffraction (XRD) results confirmed that the crystal structure of all three samples was identical with that in PDF#00−043−1002 (Powder Diffraction File). In addition, to verify successful modification, Fourier transform infrared (FT-IR) spectra were collected (Figures 1b−d). In Figure 1b, peaks for carboxylate asymmetric stretching (ν_{as} (COO^-)) and symmetric stretching (ν_s (COO^-)) from CA appeared at 1579 and 1401 cm^{-1} in CA-CeO_2, respectively. The peaks at around 1700 cm^{-1}, assigned as ν (C═O) in CA samples, were absent in CA-capped ceria due to carboxylate coordination.[31] In Figure 1c, the presence of peaks near 1660 and 1300 cm^{-1} represented stretching signals, confirming the decoration of PVP.[32] For DEX-CeO_2, bands at approximately 915 and 845 cm^{-1}, corresponding to γ (C−H) vibrations, were observed, suggesting that there were no conformational changes in the glucopyranose units, and the vibrations of glycosidic bonds were observed at 1016 and 1153 cm^{-1}. All of the peaks from the three samples were in accordance with previous works, indicating successful synthesis. Afterward, to determine the distribution of nanoceria in an aqueous solution, dynamic light scattering (DLS) was conducted. As shown in Figure 1e, nanoceria with different modifications exhibited distinct hydrodynamic diameters. Based on these results, we obtained three kinds of nanoceria with different surface coatings.

To determine which nanoceria have the potential to interact with FimH, we chose a model protein for assessment. Concanavalin A (ConA) is a lectin that has a high affinity for certain sugars, such as mannose. It has been widely used in studying glycoprotein interactions owing to its binding properties.[33] Hence, we designed a ConA aggregation assay to identify the function of ceria (Figure 1f). DLS was employed to observe the alterations in the size of the complex (Figure 1g). Following a 30 min reaction, the hydrodynamic diameter of the complex with added DEX-CeO_2 exhibited a significant increase, whereas the others demonstrated more modest growth. The DLS results proved that the existence of carbohydrates, such as DEX, could induce mannose-specific multivalent protein aggregation. Accordingly, we assumed that DEX-CeO_2 could be a potential candidate for antiadhesive nanodecoy for FimH.

Then, we selected a series of DEX derivatives with different molecular weights for optimization. As shown in Figure S3, the DECs were synthesized using a one-pot approach involving the oxidation and hydrolysis of cerium salts under basic conditions. During this process, various DEXs were employed as modifying agents (M_w = 10k, 20k, 40k, and 70k). The obtained products were named DEC10, DEC20, DEC40, and DEC70. The linear and branched structure of DEX provides a natural spatial barrier for CeO_2, preventing the growth of particles and improving the size distribution. DEC nanoparticles featuring a uniform size between 2 and 3 nm under

https://doi.org/10.1021/acsnano.3c12783
ACS Nano XXXX, XXX, XXX−XXX

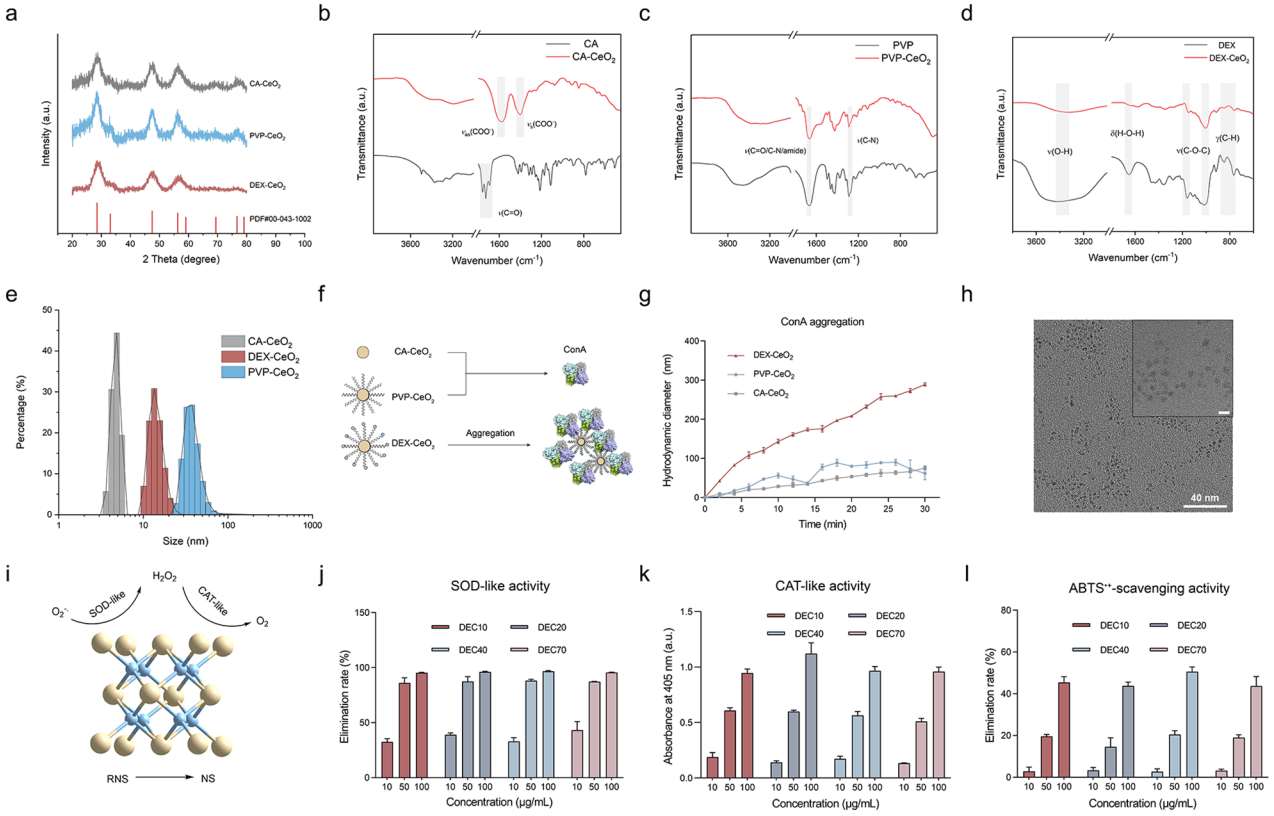

Figure 1. Characterization and antioxidant activities of DECs. (a) XRD patterns of CA-CeO_2, PVP-CeO_2, and DEX-CeO_2. FT-IR spectra of (b) CA-CeO_2, (c) PVP-CeO_2, and (d) DEX-CeO_2. (e) DLS profiles of CA-CeO_2, PVP-CeO_2, and DEX-CeO_2 (M_w = 10 kDa) in aqueous solution. (f) Mechanism of the ConA aggregation assay for screening potential nanozymes. (g) Hydrodynamic diameter changes of the ConA aggregation systems. (h) TEM images of DEX-CeO_2 (M_w = 10 kDa, the scale bar of the inset images is 5 nm). (i) Schematics of the antioxidant abilities of DECs. (j) SOD-like activities of DECs. Data are presented as the mean ± SD (n = 3). (k) CAT-like activities of DECs. Data are presented as the mean ± SD (n = 3). (l) $ABTS^{•+}$ scavenging abilities of DECs. Data are presented as the mean ± SD (n = 4).

transmission electron microscopy (TEM) (Figures 1h and S4) can be metabolized by the kidneys.[34] Due to the ultrasmall nanoscale particles and the existence of polymeric material, the XRD patterns of DECs and DEXs exhibited broadened peaks (Figure S5). Additionally, the DECs are mostly noncharged, exhibiting superior stability (Figure S6). Then, FT-IR spectra were collected to confirm the interaction between ceria and the coating. The spectra in Figure S7 indicated that the formation of DECs did not lead to conformational changes in adjacent glucopyranose units, which endowed the potential of DECs with antiadhesive activity.

ROS Scavenging Abilities of Nanodecoys. When UTIs occur, the body initiates an inflammatory response to eliminate bacteria. However, excess inflammation can cause damage to the bladder or kidneys. In this process, an excessive amount of reactive nitrogen and oxygen species (RNOS) act as proinflammatory agents, exacerbating tissue damage. Typically, superoxide anion radicals ($O_2^{•-}$) and hydrogen peroxide (H_2O_2) are representative ROS species during UTIs. DECs have excellent scavenging ability against these harmful species due to their abundant active sites (Figure 1i). Therefore, the SOD-like activity of the nanozymes was evaluated by using a SOD assay kit for WST-1, while the CAT-like activity was measured via dissolved oxygen detection and dopamine-based CAT assays.[35] As shown in Figures 1j, 1k, and S8 and S9, DECs demonstrated significant and concentration-dependent SOD- and CAT-like activities, while the DEXs showed no obvious enzymic activities. Furthermore, $ABTS^{•+}$ and $DPPH^{•}$ were selected for measuring the RNS scavenging capability of DECs (Figures 1l and S10). The reduction in absorbance of the radical cations indicated an enhanced capacity for eliminating RNS. To explore the mechanisms behind their excellent catalytic capability, X-ray photoelectron spectroscopy (XPS) analysis was conducted to examine the elemental states on the material's surface involved in catalytic reactions. The survey XPS spectra of DECs were presented in Figure S11, revealing the presence of elements such as C, O, and Ce across all spectra. Furthermore, detailed spectra for C 1*s* and O 1*s* were also gathered, providing insight into the structure and composition of all of the samples (Figures S12 and S13). More importantly, the detailed XPS spectra of Ce 3*d* revealed the valence state composition of cerium in the samples. As shown in Figure S14, the percentages of Ce^{3+} in DEC10, DEC20, DEC40, and DEC70 were 37.3%, 36.9%, 37.3%, and 32.9%, respectively. The trivalent-to-tetravalent ratio of cerium atoms in ceria determines the strength of its enzyme-like activity.[36] Such closely matched data imply a similar activity of DECs. The aforementioned results demonstrate that DECs have the potential to serve as an effective antioxidant agent for removing excessive RNOS in the inflammatory process.

***In Vitro* Anti-inflammatory and Antiadhesive Abilities of Nanodecoys.** After evaluation of the RNOS scavenging activity of DECs, their anti-inflammatory and antiadhesive abilities were investigated. A mouse macrophage line

https://doi.org/10.1021/acsnano.3c12783
ACS Nano XXXX, XXX, XXX−XXX

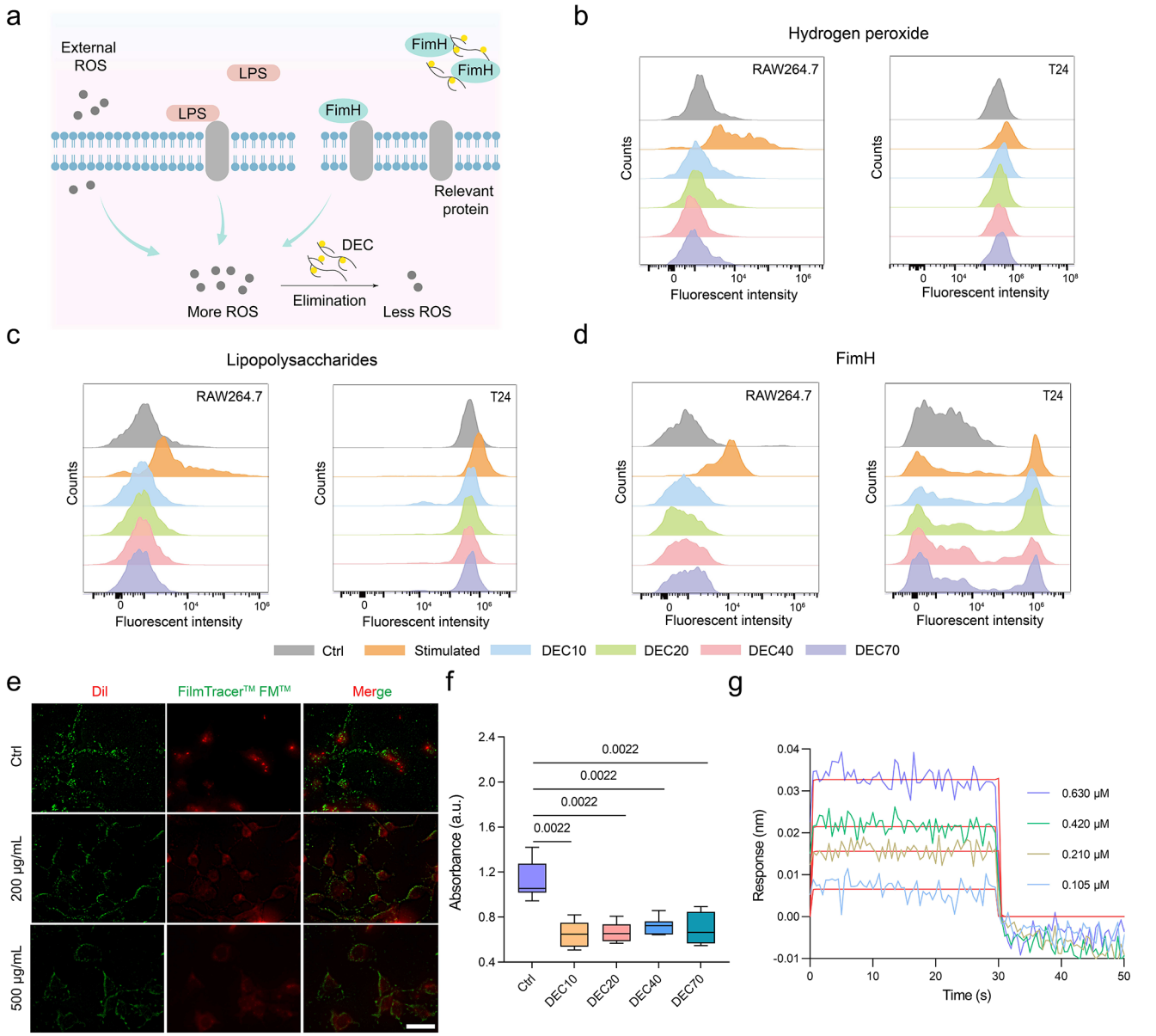

Figure 2. Antioxidant and antiadhesive abilities of DECs. (a) Schematics of DECs protecting the cell from oxidative stress. ROS levels of RAW264.7 and T24 cells were monitored by a flow cytometer in the presence or absence of DECs under (b) H_2O_2, (c) LPS, and (d) FimH stimulus. (e) Fluorescent staining images of CFT073 on T24 cells. DiI (red) and FilmTracer FM 1−43 (green) were used to stain the cell membrane of T24 and the plasma membrane of CFT073, respectively. The DECs were used at a low concentration (200 μg/mL) and a high concentration (500 μg/mL). The scale bar is 20 μm. (f) Antibiofilm formation of DECs on the abiotic surface. Data are presented as mean ± SD (n = 6). (g) BLI response of DEC40 at different concentrations.

(RAW264.7) and a human urinary bladder cancer cell line T24 (HTB-4, ATCC) were utilized as models for cellular evaluation. First, the cytotoxicity of DECs was evaluated to explore their cytocompatibility. As shown in Figures S15 and S16, DECs exhibited no toxicity toward these two types of cells and even promoted the proliferation of RAW264.7 cells, confirming their excellent biocompatibility.

Afterward, a cellular model for ROS elimination was established, and 2′,7′-dichlorodihydrofluorescein diacetate (DCFH-DA) was utilized to measure the ROS levels. To simulate the UPEC infection process, three types of stimuli were applied (Figure 2a). Hydrogen peroxide (H_2O_2), an endogenous molecule associated with inflammation, was employed to stimulate both cell types. Flow cytometry analysis demonstrated the exceptional ROS scavenging ability of DECs. In contrast, the stimulated group, that treated with H_2O_2 alone, displayed the highest fluorescence intensity in Figure 2b, indicating a significantly elevated ROS level. LPS, also known as endotoxins, are recognized by the host organism as a sign of bacterial presence. It initiates a potent immune response primarily by activating Toll-like receptor 4 (TLR4) on immune cells, resulting in the secretion of proinflammatory cytokines and other immune signaling molecules.[15] The flow cytometry results demonstrated that DECs can relieve the oxidative response caused by LPS (Figure 2c). Similar but more intuitive results were observed through laser scanning confocal microscopy (LSCM) (Figure S17). The third model was constructed with the FimH protein. The FimH protein induces inflammation by binding specifically to receptors, such as mannose receptors and TLR4.[14] The binding of FimH to these

https://doi.org/10.1021/acsnano.3c12783
ACS Nano XXXX, XXX, XXX−XXX

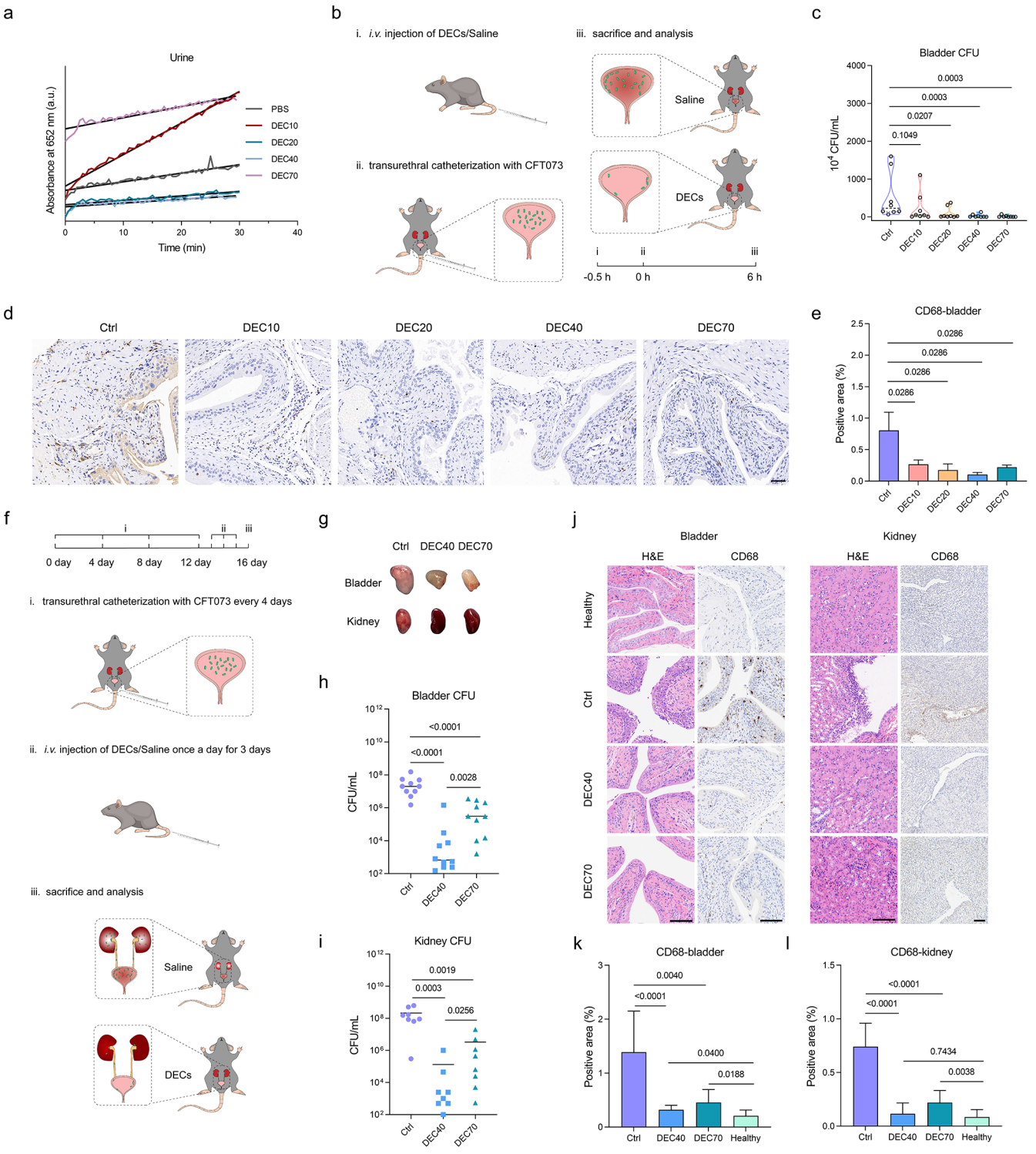

Figure 3. DECs protect bladders and kidneys in acute and repeated UTI models. (a) Signal of DECs in urine monitored by the absorbance of TMB_{ox} at 652 nm. (b) Schematics of acute UTI models. In the acute UTI model, (c) total bladder bacterial counts were determined after homogenization, and representative images of bladder sections stained with an antibody against CD68 were shown in (d). The scale bar is 50 μm. (e) Semiquantitative analysis of CD68-positive areas. Data are presented as mean ± SD (n = 4). (f) Schematics of repeated UTI models. In the repeated UTI model, representative images of bladders and kidneys with/without treatment were shown in (g), and (h) total bladder and (i) kidney bacterial counts were determined after homogenization. (j) Representative H&E staining images of bladders and kidneys. The scale bar is 100 μm. Semiquantitative analysis of CD68 positive areas in (k) bladder and (l) kidney. Data are presented as mean ± SD (n = 9 and 12, respectively).

receptors triggers a series of signaling events that contribute to the activation of immune responses and the initiation of inflammation. Before stimulation, DECs and FimH proteins were mixed and incubated. The results also indicated the

https://doi.org/10.1021/acsnano.3c12783
ACS Nano XXXX, XXX, XXX−XXX

excellent intracellular antioxidative stress capability of the nanozymes (Figures 2d and S18). It is worth noting that this outcome may stem from the inherent antioxidative activity of DECs as well as their ability to prevent FimH adhesion. These findings demonstrated that DECs have the potential to effectively combat the inflammatory storm associated with UTIs.

The interaction between host cells and UPECs plays a crucial role in UTIs. FimH-induced adhesion triggers the progression of the disease. The strain CFT073, originally isolated from a patient who suffered from UTI, was utilized to establish an infection research model.[37] Due to the excellent biocompatibility of DECs, no obvious inhibitory effects on bacterial growth were observed (Figures S19 and S20). Taking DEC40 as a representative, the adhesion of CFT073 to T24 cells was evaluated (Figure S21a). As shown in Figures 2e and S22, the amounts of CFT073 labeled with FilmTracer FM 1−43 were obviously reduced when DEC40 was coincubated, indicating that the adhesion of bacteria was prevented. Based on the experimental results above involving bacterial toxicity, it is inferred that DECs inhibited the adhesion of FimH to cells rather than killing the bacteria. Meanwhile, a bacterial aggregation assay was performed at different concentrations of DEC40. As the concentration increased, bacterial aggregation became more pronounced (Figure S23). Based on these findings, we speculated that the multivalent binding sites of DECs, upon binding to FimH, induced bacterial aggregation similar to UMOD. Taking this into consideration, we further investigated the role of DECs in preventing the formation of biofilms. As a type of adhesin, FimH is regarded as a key factor in biofilm formation under static growth conditions in a mannose-inhibitable manner, especially in implantation-like catheters.[38] To confirm whether DECs play a role in antibiofilm formation on the abiotic surface, a biofilm assay was performed and quantified via crystal violet staining (Figure S21b). As shown in Figure 2f, the formation of biofilms on plates was inhibited when DECs were applied. Based on the above-mentioned experimental results, we attempted to explore the mechanism of DECs' antiadhesive properties. Taking DEC40 as an example, we immobilized the FimH protein on a sensor for bilayer interferometry (BLI) signal analysis. As the concentration of DEC40 increased, the response signal also increased (Figure 2g). Through steady-state fitting, we estimated that the K_D value of DEC40 for FimH was 1.4 μM (Figure S24a). Furthermore, we monitored the response values of different DECs at the same concentration and found that with an increase in molecular weight, the corresponding response signal also increased (Figure S24b), which could be explained by the mechanism of multivalent enhancement.

Given the *in vitro* anti-inflammatory and antiadhesive capabilities of DECs, there will be significant potential for their use in treating UTIs.

***In Vivo* Treatment of Acute and Repeated UTIs.** From a clinical perspective, uncomplicated UTIs primarily affect individuals with no structural or neurological urinary tract abnormalities who are otherwise in good health. These infections are further divided into lower UTIs (cystitis) and upper UTIs (pyelonephritis).[2] Acute UTIs are sudden and relatively short-lived infections that affect the urinary system.

Acute UTIs are often caused by UPECs entering the urinary tract and multiplying, leading to infection. To determine the therapeutic potential of DECs for treating acute UTIs, a murine model was adapted via transurethral catheterization with CFT073. The biosafety of DECs was evaluated first. After intravenous (*i.v.*) injection of DECs three times a week, the main organs were harvested and stained with hematoxylin and eosin (H&E). All samples demonstrated negligible toxicity to the main organs at the experimental dose (Figure S25). In the meantime, murine urine was collected after 4 h of *i.v.* injection. Peroxidase-mimicking activities of DECs were used to confirm the existence of DECs metabolized from the kidneys (Figure 3a). Typically, because urine collected from different mice has varying degrees of background absorbance levels, the absorbance change of TMB_{ox} (the oxidized product of 3,3′,5,5′-tetramethylbenzidine) at 652 nm in 30 min was monitored. The signal of the DEC10 group showed an obvious increase, which implied renal clearable properties of DEC10. It is worth noting that other groups showed a weak signal change in measurement, which was attributed to the large M_w and lower concentration of DECs in urine. In addition, when disease occurs, infection and inflammation affect the renal clearable threshold and lead to different outcomes.[39] Additionally, positron emission tomography-computed tomography (PET-CT) was employed to monitor the metabolism of a nuclearly labeled substance (Figure S26). Taking DEC40 as an example, distinct signals were observed in the bladder, indicating that DEC40 could be excreted by the kidneys during the test. Combining these findings, it can be concluded that DECs can be excreted through urine.

Afterward, an acute UTI model was established through urethral bacterial injection (Figure 3b).[40] The *i.v.* injection of DECs was performed 30 min before infection. Within 6 h of treatment, bladders were harvested and homogenized. The bladders from the Ctrl group, which were not treated with DECs, showed hyperemia and edema to some degree. In contrast, the bladder status in the DEC groups was much more similar to that in the healthy group (Figure S27). We noted a significant reduction in bacteria, suggesting that DECs were effective in treating acute infection by antiadhesive therapy (Figures 3c and S28). Excess inflammation in acute UTIs can lead to various damaging effects. The H&E staining displayed significant improvements in the treatment group (Figure S29). Then, CD68 was stained to evaluate the macrophage count (Figure 3d and 3e). In the Ctrl group, high CD68-positive areas were observed. After administration of DECs, the expression of CD68 was lower, indicating an improved state and demonstrating that DECs can scavenge inflammation. With the treatment of DECs, oxidative stress was relieved. It is noted that while DEC10 and DEC20 showed promising results in terms of anti-inflammation, their performance in bacterial elimination was suboptimal. This could be attributed to their relatively smaller molecular weight, leading to rapid metabolism under pathological conditions and inadequate reduction in bacterial content. Therefore, in subsequent experiments, we employed DEC40 and DEC70 for treatment.

After an initial urinary tract infection, almost 20−30% of women with a UTI will have a second UTI within 6 months, while 3% of them will experience a third UTI during that time period.[41] Repeated UTIs refer to instances where an individual experiences UTIs multiple times. After verifying the antiadhesive and anti-inflammatory abilities of DECs in the acute UTI model, we constructed a repeated model through multiple infections in mice (Figure 3f). Correspondingly, the dosage of the DEC treatment was also increased. Because UPECs exhibit the ability to inhabit various regions within the urinary tract,

https://doi.org/10.1021/acsnano.3c12783
ACS Nano XXXX, XXX, XXX−XXX

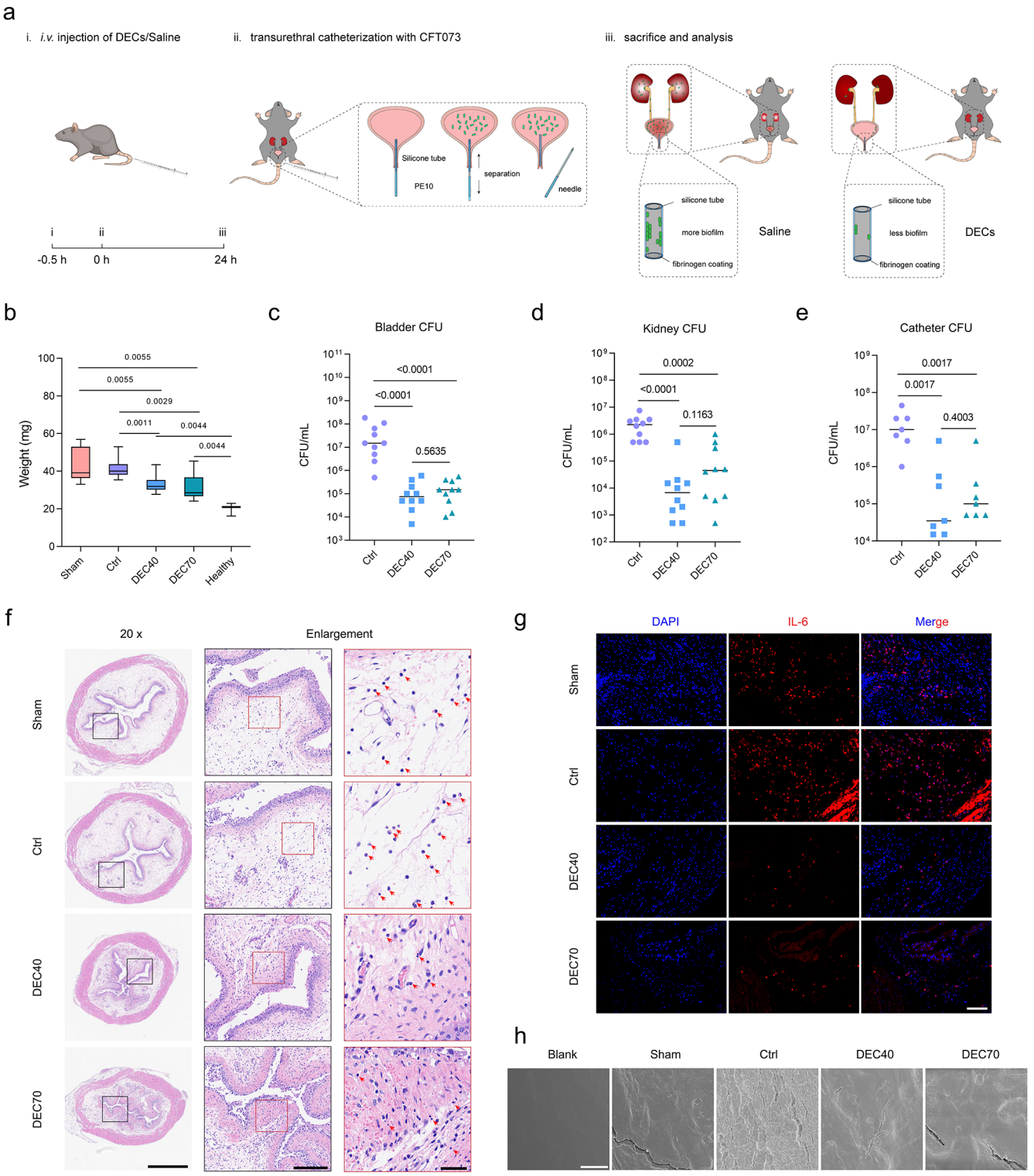

Figure 4. DECs protect bladders and kidneys in CAUTI models. (a) Schematics of CAUTI models. (b) Weight of the bladders in the CAUTI model. The data are shown as the means ± SDs (for the sham group, $n = 8$; healthy group, $n = 3$; other groups, $n = 12$). (c–e) Total bladder/kidney/catheter bacterial counts. (f) Bladder H&E staining images of the Ctrl and treatment groups. Red arrows indicate neutrophil leukocytes and other inflammation-related cells. The scale bars are 1 mm, 200 μm, and 50 μm. (g) Representative images of bladder sections stained with an IL-6 antibody. The scale bar is 100 μm. (h) Representative SEM images of catheters in the Ctrl and treatment groups. The scale bar is 10 μm.

encompassing the urethra, ureters, kidneys, and bladders, we collected the kidneys and bladders for further investigation. As shown in Figures 3g and S30, extensive abscess of the kidney was observed in the Ctrl group, while the two treatment groups showed less area related to tissue pathology. The status of the bladders was similar to that in the acute model. These results

https://doi.org/10.1021/acsnano.3c12783
ACS Nano XXXX, XXX, XXX−XXX

might be attributed to serious infection and a hyperactive innate immune response. We assessed the amounts of bacteria in these two organs. Both DEC40 and DEC70 groups demonstrated effectiveness in eradicating bacteria from the bladders and kidneys (Figures 3h, 3i, S31) while also mitigating inflammatory responses (Figures 3j–l, S32, and S33). To explore the alterations in the ROS levels following treatments with DECs, dihydroethidium (DHE) was applied for evaluate the ROS levels in bladders. As shown in Figure S34, the treatment group demonstrated weaker fluorescent signal, while the Ctrl group showed more which indicated antioxidant abilities of DECs. In addition, we evaluated the level of fibrosis in infected kidneys using Masson's trichrome (MT) staining (Figure S35). The severity of renal fibrosis signifies the inadequacy of kidney function. DECs protect the kidney from fibrosis, which is attributed to their excellent anti-inflammatory and antiadhesive activities.

***In Vivo* Treatment of Catheter-Associated UTIs.** The other kind of UTI is complicated UTIs, which are characterized by factors that compromise the urinary tract or host defense mechanisms. Catheter-associated UTIs (CAUTIs) are particularly concerning because they lead to increased morbidity and mortality, representing the most common cause of secondary bloodstream infections.[42]

To explore whether treatment with DECs is effective for CAUTIs, we established a CAUTI model using medical silicone tubing (Figure 4a). Implanting tubing into the bladder leads to histological and immunological alterations in the bladder of mice.[43,44] Specifically, the introduction of a urinary catheter disrupts the protective layers of the uroepithelium and results in observable histological modifications. As mentioned above, all the groups exhibited varying degrees of edema due to implant existence. The presence of bacteria and an excess inflammatory response exacerbated the phenomenon of edema. Encouragingly, the weight of bladders treated with DECs was decreased, indicating that edema was relieved (Figure 4b). Then, we counted the bacteria in the bladders, kidneys, and catheters. As shown in Figures 4c–e, after treatment, there was a significant reduction in the quantity of bacteria. Meanwhile, H&E staining (Figures 4f and S37) and CD68 staining (Figure S38) of the two organs both demonstrated the bioprotective effects of DECs against inflammation storms. During the acute infection process, the infiltration of central granulocytes and other immune cells in response was significantly reduced (Figure 4f). The same results also appeared in the IL-6 immunofluorescence-stained samples (Figures 4g, S39, and S40). In addition to the organ results, the white blood cell (WBC) counts and the proportion of lymphocytes (Lymph%) also indicated decreased inflammation in the blood (Figure S41). Furthermore, edema was particularly evident in the slices (Figures 4f and S38), consistent with the trend observed in the previous qualitative results of bladders. The physiologic response to catheterization also includes the release of fibrinogen that coats the catheter surface.[2,43] In all groups, we observed coatings that might be fibrinogen inside of the silicone tubing (Figure 4h). The Ctrl group showed significant biofilm formation, while the treatment group exhibited better conditions, which was consistent with the results of the *in vitro* experiment. According to catheter-associated mouse models, DECs showed great potential in ameliorating UTIs from potential bacterial infection by effective ROS scavenging and antiadhesive activities. It provides a viable option for eradicating infections related to implants.

CONCLUSION

In conclusion, we engineered ultrasmall ceria nanoparticles coated with dextran to mimic the UMOD function for UTI treatment. The dextran component serves as a multivalent decoy, obstructing the adhesion of FimH proteins, while the ceria component exhibits excellent anti-inflammatory properties. These ultrasmall particles are designed to be metabolized by the kidneys, effectively reducing bacterial colonization in both the upper and lower urinary tracts. This dual-action approach alleviates excessive inflammation and mitigates further tissue damage. As a result of these integrated functionalities, DECs have been proven to be effective in alleviating acute UTIs, repeated infections, and CAUTIs in a mouse model. This bioinspired study not only illustrated antiadhesive nanozymes to protect urinary tissue from external bacteria but also reduced the potent risk of excess inflammation.

METHODS

Synthesis of Nanoceria with Different Modifications. Synthesis of CA-CeO_2: To prepare CA-ceria NPs, citric acid (0.48 g) and cerium nitrate pentahydrate (0.52 g) were dissolved in water (30 mL) and rapidly poured into 100 mL of a 3 M ammonia solution. The mixed solution was stirred overnight at 25 °C, centrifuged, and washed with water.[45]

Synthesis of PVP-CeO_2: $Ce(NO_3)_3{\cdot}6H_2O$ (0.2 mmol) was dissolved in a PVP ethanol solution (40 mL, 30 g/L). Then, triethylamine (2 mmol) was added dropwise to the Ce^{3+} solution. The stock solution was transferred into a Teflon bottle, held tightly in a stainless-steel vessel and then heated at 180 °C for 24 h. After being cooled to room temperature, the reaction solution was separated and washed with water-acetone mixed solvent (v/v = 1:10).[46]

Synthesis of DEX-CeO_2: First, dextran with different molecular weights was dissolved in 10 mL of deionized water, followed by several minutes of sonication to get a homogeneous solution (1.0 M, marked as solution A). Then, 5 mL of $Ce(NO_3)_3{\cdot}6H_2O$ liquor (1.0 M, solution B) was added to solution A. The solution was vortexed for 3 min and then added dropwise to 30 mL of $NH_3{\cdot}H_2O$ to form suspension C under vigorous stirring. After this, suspension C was stirred at room temperature for 24 h. To keep the chain concentration the same, different masses of dextran were adopted.[47]

ConA Aggregation Assay. ConA as a model protein has been widely used for studying carbohydrate–protein interaction.[48] The ConA has a high affinity for certain carbohydrate like mannose. In the given buffers (pH = 7.04, 10 mM Ca^{2+} and Mn^{2+}), the ConA exists predominantly as a tetramer of four identical subunits.[49] The tetramer provided four binding sites for carbohydrate. When the tetramer met the multivalent carbohydrate, the interactions would induce aggregation. And this aggregation could be detected by DLS. Typically, a series of mixtures (2.0 mL) of Con A (500 μL, 4 μM) and ceria (40 μL, 1 mg/mL) in a buffer solution (10 mM PBS, 0.1 mM $MnCl_2$, and 0.1 mM $CaCl_2$; pH 7.04) were equilibrated at room temperature and monitored by DLS for 30 min.

Measurement of Enzymatic Activities. To determine the superior RNOS scavenging abilities of DEC nanozymes, we checked SOD-like activities to eliminate $O_2^{\bullet-}$, CAT-like activities to remove H_2O_2 and RNS scavenging activities against reactive nitrogen analogs (2,2′-azinobis (3-ethyl benzothi-azoline-6-sulfonic acid) ammonium radical ($ABTS^{\bullet+}$) and 1,1-diphenyl-2-picryl-hydrazyl radical ($DPPH^{\bullet}$)).

Measurement of SOD-like activities: The SOD-like activities of DECs were tested via an SOD assay kit according to the protocols of the assay kit. Typically, different DEC samples were serially diluted and mixed with 200 μL of a WST-1 (2-(4-iodophenyl)-3-(4-

https://doi.org/10.1021/acsnano.3c12783
ACS Nano XXXX, XXX, XXX–XXX

nitrophenyl)-5-(2,4-disulfophenyl)-2H tetrazolium sodium salt) probe solution. Following enzyme solution addition to start the reaction, the system was incubated at 37 °C for 20 min. The absorbance at 450 nm was recorded by a microplate reader. The final concentrations of the DEC nanozymes were 10, 50, and 100 μg/mL.

Measurement of CAT-like activities: The CAT-like activities of DECs were evaluated by detecting oxygen production from H_2O_2 in solution with a dissolved oxygen meter. Normally, different concentrations of DECs were mixed with 5.0 mM H_2O_2 in an aqueous solution. The change in dissolved oxygen concentration over 5 min was recorded. Additionally, the CAT-like activities were also evaluated by a dopamine-based assay. In a typical measurement, the reaction system in the 96-well plate contained 5 μL of DECs, 90 μL of Tris buffer (10 mM, pH 8.5), 100 μL of DA (2 mg/mL), and 5 μL of H_2O_2 (0.8 M). After adding the solution into the plate, the plate was quickly transferred to the anaerobic device and incubated at 37 °C for 10 min. Finally, the absorbance at 405 nm was recorded by using a microplate spectrophotometer.[35]

Measurement of $ABTS^{\bullet+}$-scavenging abilities: First, 10 mL of ABTS (7 mM) and 10 mL of $K_2S_2O_8$ (2.45 mM) aqueous solution were premixed, and the mixed solution was stored in the dark overnight to obtain an $ABTS^{\bullet+}$ mother solution. The working solution contained 50 μL of ABTS mother liquor, 100 μL of DEC solution, and 850 μL of 1 × PBS. The final concentrations of DEC nanozyme were 10, 50, and 100 μg/mL. The mixture was incubated at 37 °C, and the absorbance at 734 nm was recorded by using a microplate reader.

Measurement of $DPPH^{\bullet}$ scavenging abilities: First, 1.50 mg of DPPH was dissolved in 15 mL of methanol. Due to the insolubility of DEC in methanol, an aqueous solution was used. The working solution contained 50 μL of DPPH-methanol solution, 100 μL of DEC solution, and 850 μL of 1 × PBS. The mixture was incubated at 37 °C, and the absorbance at 517 nm was recorded using a microplate reader.

Cell Culture. A mouse macrophage line (RAW264.7) was cultured in DMEM, and the human urinary bladder cancer cell line T24 (HTB-4, ATCC) was cultured in McCoy's 5A medium. Both of these were supplemented with 10% fetal bovine serum (FBS), penicillin, and streptomycin. All cells were incubated at 37 °C in a humidified atmosphere containing 5% CO_2 in air.

***In Vitro* Cytotoxicity Evaluation.** RAW264.7 and T24 cells were cultured in 96-well plates (1.0×10^4 cells per well) in 100 μL of DMEM or McCoy's 5A medium with 10% FBS, 1% penicillin, and streptomycin. After overnight culture, the cells were treated with various doses of DECs. Cell viability was monitored by a cell counting kit-8 assay after 24 h of treatment.

***In Vitro* Antioxidant and Anti-inflammatory Evaluation.** Since microorganism infection is accompanied by endotoxin release and protein stimulation, LPS and FimH were chosen to establish an oxidative stress model. In addition, H_2O_2 was adopted as excess ROS produced during hyperactive innate immunity. The intracellular ROS level was evaluated by using DCFH-DA as a fluorescent probe through flow cytometry and laser scanning confocal microscopy.

Typically, RAW264.7 cells were incubated with a 6-well plate at 37 °C for 24 h, and the density of each well was 1×10^5. Then, 50 μg/mL DECs were added to each well plate for another 2 h. After washing the cells several times with 1 × PBS, 1 μg/mL LPS was added and incubated for an hour. After that, DCFH-DA (0.01 mM) in DMEM was added to each well plate for 30 min followed by washing. The fluorescence images were recorded using laser scanning confocal microscopy. Flow cytometry was performed for semiquantitative analysis. Similarly, T24 cells were treated as mentioned above with flow cytometry.

For the FimH segment, before the simulation, FimH protein (10 μg/mL) and DECs were incubated for 2 h. RAW264.7 cells were incubated with a 6-well plate at 37 °C for 12 h, and the density of each well was 1×10^5. Then, the mixed solution was added to each well plate for another 4 h. After washing the cells several times with 1 × PBS, DCFH-DA (0.01 mM) in DMEM was added to each well plate for 30 min followed by washing. The fluorescence images were recorded using laser scanning confocal microscopy. Flow cytometry was performed for semiquantitative analysis. Similarly, T24 cells were treated as mentioned above with flow cytometry.

For the H_2O_2 segment, the basic operation was the same as that for the LPS group, except 0.08 mM H_2O_2 was added as a simulator. Two cell lines were handled and analyzed by using flow cytometry.

Bacterial Viability. CFT073 viability was determined by monitoring the absorbance at 600 nm. DECs were added, and the final concentration was determined to be 1 mg/mL. After 18 h of incubation, the absorbance of all groups was recorded. In addition, DEC40 was chosen to evaluate the bacterial viability at other concentrations.

Adhesion Assay. The adhesion of CFT073 to T24 cells was evaluated following the method described by Hawdon et al. with some modifications.[50] T24 cells were grown in 12-well plates for 12 h. Then, the cells were stained with Dil (10 μM) for 20 min to label the cell membranes. Then, the cells were washed with PBS. After being serum starved for 2 h, the cells were inoculated with a bacterial suspension. Before the infection experiment, CFT073 was stained with FilmTracer FM 1−43 for 30 min under dark conditions. After being washed three times with sterile 0.9% NaCl solution, bacterial pellets were suspended in serum-free McCoy's 5A without antibiotics and adjusted to 1×10^7 CFU/mL prior to the adherence assay. T24 cells were treated with DEC40 for 15 min and seeded with 50 μL of an OD = 0.1 bacterial suspension for 30 min. Following incubation, the monolayers were washed with PBS, and the adhered bacteria were determined by epifluorescence microscopy.

Light Microscopy of DEC40 and CFT073. CFT073 was grown in M9 media supplemented with 0.01 mg/mL biotin, 0.01 mg/mL thiamine, 0.01 mg/mL amino acid mix (containing all L-natural amino acids, except glutamine, in ddH_2O), and 0.4% glucose. At OD600 = 1, cells were then harvested at 2700*g* for 5 min, resuspended in M9 media without glucose, and incubated for 1 h at 37 °C with mild shaking (350 rpm). Ninety microliters of OD600 = 0.9 cells were mixed with DEC40 solution to final concentrations of 0, 0.35, and 1.76 mg/mL. Reactions were incubated for 2 h at 37 °C with shaking. Aliquots of 5 μL from each reaction mixture were spotted and covered with a coverslip, and random images were collected with a 40 × objective.[6]

Biofilm Assay. CFT073 was grown in LB in wells of PVC microtiter plates at 23 °C in the presence of DECs at varying concentrations. After 24 h of growth, the wells were rinsed with water and stained with crystal violet for quantification.

Biolayer Interferometry (BLI) Assay. The Octet K2 system (Molecular Device, ForteBIO, USA) was used for the characterization of protein−ligand binding affinity. The recombinant protein FimH (10 μg/mL) was immobilized on an Octet Ni-NTA biosensor. The sensors were then stabilized and moved into wells containing various concentrations of the test compounds in a kinetic buffer (PBST). Buffer was added to a 96-well plate, and the plate was transferred to the K2 instrument for analysis by running it serially at 30 °C with a shaking speed of 1000 rpm. Baseline readings were obtained in buffer (60 s), associations were obtained in wells containing compound (30 s), and dissociation was observed in buffer (30 s). After interference from the sensor and ligand-containing buffers was removed, the binding signals were identified, and the results were analyzed using OctetHT V10.0 software. Then, the affinity constant (K_D) values were calculated by steady-state fitting.

Animals. All animal experiments were approved by the Institutional Animal Care and Use Committee (IACUC) of Nanjing University. Female C57BL/6J mice (6−8 weeks) were supplied by Beijing Vital River Laboratory Animal Technology Co., Ltd. (China). After acclimatization for 7 days, the mice were subjected to different experiments.

Renal Clearance Studies of Ultrasmall DECs. Renal clearance studies of DECs were determined via urine catalytic activity assays. The urine was collected until 4 h of *i.v.* injection. For all assays, 20 μL of urine was diluted to 80 μL at pH = 4.0 HAc-NaAc buffer and allowed to equilibrate at room temperature for 15 min. Then, 100 μL of 10 mM TMB, 20 μL of 1 M H_2O_2, and 780 μL of the buffer

https://doi.org/10.1021/acsnano.3c12783
ACS Nano XXXX, XXX, XXX−XXX

solution were added. After 5 min of reaction, the plate was read kinetically at 652 nm over the course of 30 min.

***In Vivo* Antiadhesive and Anti-inflammatory Ability Evaluation.** *In vivo* antiadhesive and anti-inflammatory evaluations were conducted in three types of UTI models.[13,40,44] CFT073 was chosen as an infectional pathogen, and the bacteria were grown under type 1 pilus-inducing conditions (2 × 24 h at 37 °C statically in LB). C57BL/6J mice were used due to their strong innate inflammatory response.

In the acute UTI model, eight-week-old C57BL/6J female mice in the treatment groups were *i.v.* injected with DECs at 8 mg/kg, while the control group was treated with saline. Thirty minutes later, all groups were anesthetized by inhalation of isoflurane and infected via transurethral catheterization with 60 μL of the bacterial suspension, resulting in 1×10^7 to 2×10^7 inoculum. At 6 h after infection, the mice were killed by cervical dislocation under anesthesia, and the bladders were immediately harvested and processed.

In the repeated UTI model, 7- to 8-week-old female mice were anesthetized by inhalation of isoflurane and infected via transurethral catheterization with 60 μL of bacterial suspension, resulting in 1×10^7 to 2×10^7 inoculum. After repeated infection every 3 days 4 times, DECs were *i.v.* injected every day 3 times. After that, the mice were killed by cervical dislocation under anesthesia and the bladders and kidneys were collected.

In the CAUTI model, nanozymes were *i.v.* injected before infection. Then, 7- to 8-week-old female mice were anesthetized by inhalation of isoflurane and implanted with a 4- to 5 mm length of biomedical silicone tubing. Immediately following implantation, 60 μL of the bacterial suspension (1×10^7 to 2×10^7 CFU) in phosphate-buffered saline (PBS) was introduced into the bladder lumen by transurethral inoculation. At 24 h after infection, the mice were killed by cervical dislocation under anesthesia, and the bladders, kidneys, and catheters were collected. In catheter-associated UTIs models, the Sham group represents the mice were implanted with catheter but not infected, while the Ctrl group means the mice were implanted with catheter and infected with CFT073.

Bacterial Titer Determination on Implants and Organs. Animals were sacrificed at the indicated time points by cervical dislocation after anesthesia inhalation, and the bladders and kidneys were aseptically harvested. Subsequently, the silicone implant was retrieved from the bladder when present, placed in PBS, sonicated for 10 min, and then vortexed at a maximum speed for 3 min. The bladder and kidneys of each mouse were homogenized in PBS. Samples were serially diluted and plated onto LB agar plates. CFU were enumerated after 24 h of incubation at 37 °C.

Histopathology. For histological analyses, bladders and kidneys were fixed in formalin at room temperature. They were then embedded in paraffin, sectioned, and stained with hematoxylin and eosin (H&E) and Masson's trichrome. For the immunohistochemical and immunofluorescent analysis, tissue sections were incubated with antibodies against CD68 and IL-6. ImageJ software was used for the semiquantitative analysis of histological images.

Statistical Analysis. Data were shown as mean ± SD. Statistical analysis to compare median values between groups was determined by Mann–Whitney U test.

ASSOCIATED CONTENT

Supporting Information

The Supporting Information is available free of charge at https://pubs.acs.org/doi/10.1021/acsnano.3c12783.

Chemicals and reagents, instrumentations, material characterization (XRD, TEM, Zeta potential, FT-IR, and XPS), enzymic activities, *in vitro* efficacy evaluation (cytotoxicity, antioxidant/antiadhesive ability of nanozymes), and *in vivo* efficacy evaluation (biocompatibility, biodistribution, anti-inflammation, and antiadhesion ability of nanozymes) are described (Figures S1–S41, Table S1) (PDF)

AUTHOR INFORMATION

Corresponding Author

Hui Wei − *College of Engineering and Applied Sciences, Nanjing National Laboratory of Microstructures, Jiangsu Key Laboratory of Artificial Functional Materials and State Key Laboratory of Analytical Chemistry for Life Science, School of Chemistry and Chemical Engineering, Chemistry and Biomedicine Innovation Center (ChemBIC), Nanjing University, Nanjing, Jiangsu 210023, China; NMPA Key Laboratory for Biomedical Optics, Hangzhou, Zhejiang 310018, China;* orcid.org/0000-0003-0870-7142; Email: weihui@nju.edu.cn

Authors

Yihong Zhang − *College of Engineering and Applied Sciences, Nanjing National Laboratory of Microstructures, Jiangsu Key Laboratory of Artificial Functional Materials, Nanjing University, Nanjing, Jiangsu 210023, China*

Wanling Liu − *College of Engineering and Applied Sciences, Nanjing National Laboratory of Microstructures, Jiangsu Key Laboratory of Artificial Functional Materials, Nanjing University, Nanjing, Jiangsu 210023, China*

Gen Wei − *College of Engineering and Applied Sciences, Nanjing National Laboratory of Microstructures, Jiangsu Key Laboratory of Artificial Functional Materials, Nanjing University, Nanjing, Jiangsu 210023, China*

Quanyi Liu − *State Key Laboratory of Electroanalytical Chemistry, Changchun Institute of Applied Chemistry, Chinese Academy of Sciences, Changchun, Jilin 130022, China; School of Applied Chemistry and Engineering, University of Science and Technology of China, Hefei, Anhui 230026, China*

Guoqiang Shao − *Department of Nuclear Medicine, Nanjing First Hospital, Nanjing Medical University, Nanjing, Jiangsu 210006, China*

Xiang Gu − *College of Engineering and Applied Sciences, Nanjing National Laboratory of Microstructures, Jiangsu Key Laboratory of Artificial Functional Materials, Nanjing University, Nanjing, Jiangsu 210023, China*

Xiaomiao Cui − *College of Engineering and Applied Sciences, Nanjing National Laboratory of Microstructures, Jiangsu Key Laboratory of Artificial Functional Materials, Nanjing University, Nanjing, Jiangsu 210023, China*

Zijun Zhou − *College of Engineering and Applied Sciences, Nanjing National Laboratory of Microstructures, Jiangsu Key Laboratory of Artificial Functional Materials, Nanjing University, Nanjing, Jiangsu 210023, China*

Yuting Wang − *College of Engineering and Applied Sciences, Nanjing National Laboratory of Microstructures, Jiangsu Key Laboratory of Artificial Functional Materials, Nanjing University, Nanjing, Jiangsu 210023, China*

Sheng Zhao − *College of Engineering and Applied Sciences, Nanjing National Laboratory of Microstructures, Jiangsu Key Laboratory of Artificial Functional Materials, Nanjing University, Nanjing, Jiangsu 210023, China; Key Laboratory of Advanced Drug Delivery Systems of Zhejiang Province, College of Pharmaceutical Sciences, Zhejiang University, Hangzhou, Zhejiang 310058, China*

Faheem Muhammad − *College of Engineering and Applied Sciences, Nanjing National Laboratory of Microstructures, Jiangsu Key Laboratory of Artificial Functional Materials, Nanjing University, Nanjing, Jiangsu 210023, China*

https://doi.org/10.1021/acsnano.3c12783
ACS Nano XXXX, XXX, XXX−XXX

Sirong Li − *College of Engineering and Applied Sciences, Nanjing National Laboratory of Microstructures, Jiangsu Key Laboratory of Artificial Functional Materials, Nanjing University, Nanjing, Jiangsu 210023, China*
Tong Li − *College of Engineering and Applied Sciences, Nanjing National Laboratory of Microstructures, Jiangsu Key Laboratory of Artificial Functional Materials, Nanjing University, Nanjing, Jiangsu 210023, China*
Yan Du − *State Key Laboratory of Electroanalytical Chemistry, Changchun Institute of Applied Chemistry, Chinese Academy of Sciences, Changchun, Jilin 130022, China; School of Applied Chemistry and Engineering, University of Science and Technology of China, Hefei, Anhui 230026, China;* orcid.org/0000-0003-3197-7204

Complete contact information is available at: https://pubs.acs.org/10.1021/acsnano.3c12783

Author Contributions

#Y.Z. and W.L. contributed equally.

Funding

This work was funded by the National Natural Science Foundation of China (22374071), the National Key R&D Program of China (2021YFF1200700and 2019YFA0709200), Jiangsu Provincial Key R&D Program (BE2022836), the PAPD Program, State Key Laboratory of Analytical Chemistry for Life Science (5431ZZXM2306), NMPA Key Laboratory for Biomedical Optics (20240001), and Fundamental Research Funds for the Central Universities (202200325, 021314380228, and 021314380195).

Notes

The authors declare no competing financial interest.

ACKNOWLEDGMENTS

We would like to express our gratitude to Prof. Chao Yan for his assistance with FimH protein. We used OpenAI for general grammar check and occasional polishing in both manuscript and supporting files.

REFERENCES

(1) Foxman, B. The Epidemiology of Urinary Tract Infection. *Nat. Rev. Urol* **2010**, *7* (12), 653−660.
(2) Flores-Mireles, A. L.; Walker, J. N.; Caparon, M.; Hultgren, S. J. Urinary Tract Infections: Epidemiology, Mechanisms of Infection and Treatment Options. *Nat. Rev. Microbiol* **2015**, *13* (5), 269−284.
(3) Klein, R. D.; Hultgren, S. J. Urinary Tract Infections: Microbial Pathogenesis, Host-pathogen Interactions and New Treatment Strategies. *Nat. Rev. Microbiol* **2020**, *18* (4), 211−226.
(4) Hung, C. S.; Bouckaert, J.; Hung, D.; Pinkner, J.; Widberg, C.; DeFusco, A.; Auguste, C. G.; Strouse, R.; Langermann, S.; Waksman, G.; et al. Structural Basis of Tropism of Escherichia Coli to the Bladder During Urinary Tract Infection. *Mol. Microbiol.* **2002**, *44* (4), 903−915.
(5) Devuyst, O.; Olinger, E.; Rampoldi, L. Uromodulin: From Physiology to Rare and Complex Kidney Disorders. *Nat. Rev. Nephrol* **2017**, *13* (9), 525−544.
(6) Weiss, G. L.; Stanisich, J. J.; Sauer, M. M.; Lin, C. W.; Eras, J.; Zyla, D. S.; Truck, J.; Devuyst, O.; Aebi, M.; Pilhofer, M.; et al. Architecture and Function of Human Uromodulin Filaments in Urinary Tract Infections. *Science* **2020**, *369* (6506), 1005−1010.
(7) Hartmann, M.; Lindhorst, T. K. The Bacterial Lectin FimH, a Target for Drug Discovery - Carbohydrate Inhibitors of Type 1 Fimbriae-Mediated Bacterial Adhesion. *Eur. J. Org. Chem.* **2011**, *2011* (20−21), 3583−3609.
(8) Hatton, N. E.; Baumann, C. G.; Fascione, M. A. Developments in Mannose-Based Treatments for Uropathogenic Escherichia coli-induced Urinary Tract Infections. *Chembiochem* **2021**, *22* (4), 613−629.
(9) Richards, S. J.; Fullam, E.; Besra, G. S.; Gibson, M. I. Discrimination Between Bacterial Phenotypes Using Glyco-nanoparticles and the Impact of Polymer Coating on Detection Readouts. *J. Mater. Chem. B* **2014**, *2* (11), 1490−1498.
(10) Ting, S. R. S.; Min, E. H.; Zetterlund, P. B.; Stenzel, M. H. Controlled/Living ab Initio Emulsion Polymerization via a Glucose RAFTstab: Degradable Cross-Linked Glyco-Particles for Concanavalin A/FimH Conjugations to Cluster E. coli Bacteria. *Macromolecules* **2010**, *43* (12), 5211−5221.
(11) Pasparakis, G.; Alexander, C. Sweet Talking Double Hydrophilic Block Copolymer Vesicles. *Angew. Chem. Int. Edit* **2008**, *47* (26), 4847−4850.
(12) Spaulding, C. N.; Klein, R. D.; Ruer, S.; Kau, A. L.; Schreiber, H. L.; Cusumano, Z. T.; Dodson, K. W.; Pinkner, J. S.; Fremont, D. H.; Janetka, J. W.; et al. Selective Depletion of Uropathogenic E. coli from the Gut by a FimH Antagonist. *Nature* **2017**, *546* (7659), 528−532.
(13) Cusumano, C. K.; Pinkner, J. S.; Han, Z. F.; Greene, S. E.; Ford, B. A.; Crowley, J. R.; Henderson, J. P.; Janetka, J. W.; Hultgren, S. J. Treatment and Prevention of Urinary Tract Infection with Orally Active FimH Inhibitors. *Sci. Transl Med.* **2011**, *3* (109), 109ra115.
(14) Ashkar, A. A.; Mossman, K. L.; Coombes, B. K.; Gyles, C. L.; Mackenzie, R. FimH Adhesin of Type 1 Fimbriae Is a Potent Inducer of Innate Antimicrobial Responses Which Requires TLR4 and Type 1 Interferon Signalling. *Plos Pathog* **2008**, *4* (12), e1000233.
(15) Aderem, A.; Ulevitch, R. J. Toll-like Receptors in the Induction of the Innate Immune Response. *Nature* **2000**, *406* (6797), 782−787.
(16) Kohanski, M. A.; Dwyer, D. J.; Collins, J. J. How Antibiotics Kill Bacteria: From Targets to Networks. *Nat. Rev. Microbiol* **2010**, *8* (6), 423−435.
(17) VanHook, A. M. Antibiotic-induced Inflammation. *Sci. Signal.* **2022**, *15* (745), eade1683.
(18) Hannan, T. J.; Mysorekar, I. U.; Hung, C. S.; Isaacson-Schmid, M. L.; Hultgren, S. J. Early Severe Inflammatory Responses to Uropathogenic E-coli Predispose to Chronic and Recurrent Urinary Tract Infection. *Plos Pathog* **2010**, *6* (8), e1001042.
(19) Wu, J. J. X.; Wang, X. Y.; Wang, Q.; Lou, Z. P.; Li, S. R.; Zhu, Y. Y.; Qin, L.; Wei, H. Nanomaterials with Enzyme-like Characteristics (Nanozymes): Next-Generation Artificial Enzymes (II). *Chem. Soc. Rev.* **2019**, *48* (4), 1004−1076.
(20) Huang, Y. Y.; Ren, J. S.; Qu, X. G. Nanozymes: Classification, Catalytic Mechanisms, Activity Regulation, and Applications. *Chem. Rev.* **2019**, *119* (6), 4357−4412.
(21) Wei, H.; Gao, L. Z.; Fan, K. L.; Liu, J. W.; He, J. Y.; Qu, X. G.; Dong, S. J.; Wang, E. K.; Yan, X. Y. Nanozymes: A Clear Definition with Fuzzy Edges. *Nano Today* **2021**, *40*, 101269.
(22) Liang, M. M.; Yan, X. Y. Nanozymes: From New Concepts, Mechanisms, and Standards to Applications. *Acc. Chem. Res.* **2019**, *52* (8), 2190−2200.
(23) Liu, W. L.; Zhang, Y. H.; Wei, G.; Zhang, M. X.; Li, T.; Liu, Q. Y.; Zhou, Z. J.; Du, Y.; Wei, H. Integrated Cascade Nanozymes with Antisenescence Activities for Atherosclerosis Therapy. *Angew. Chem. Int. Edit* **2023**, *62*, e202304465.
(24) Xi, J.; Zhang, R.; Wang, L.; Xu, W.; Liang, Q.; Li, J.; Jiang, J.; Yang, Y.; Yan, X.; Fan, K.; Gao, L. A Nanozyme-Based Artificial Peroxisome Ameliorates Hyperuricemia and Ischemic Stroke. *Adv. Funct. Mater.* **2021**, *31* (9), 2007130.
(25) Zhang, Y.; Khalique, A.; Du, X. C.; Gao, Z. X.; Wu, J.; Zhang, X. Y.; Zhang, R.; Sun, Z. Y.; Liu, Q. Q.; Xu, Z. L.; et al. Biomimetic Design of Mitochondria-Targeted Hybrid Nanozymes as Superoxide Scavengers. *Adv. Mater.* **2021**, *33* (9), 2006570.
(26) Liu, Y. F.; Cheng, Y.; Zhang, H.; Zhou, M.; Yu, Y. J.; Lin, S. C.; Jiang, B.; Zhao, X. Z.; Miao, L. Y.; Wei, C. W.; et al. Integrated Cascade Nanozyme Catalyzes in vivo ROS Scavenging for Anti-inflammatory Therapy. *Sci. Adv.* **2020**, *6* (29), eabb2695.

(27) Kim, Y. G.; Lee, Y.; Lee, N.; Soh, M.; Kim, D.; Hyeon, T. Ceria-Based Therapeutic Antioxidants for Biomedical Applications. *Adv. Mater.* **2023**, 2210819.
(28) Heinze, T.; Liebert, T.; Heublein, B.; Hornig, S. Functional Polymers Based on Dextran. *Polysaccharides ll* **2006**, *205*, 199−291.
(29) Barghouthi, S.; Guerdoud, L. M.; Speert, D. P. Inhibition by Dextran of Pseudomonas Aeruginosa Adherence to Epithelial Cells. *Am. J. Respir* **1996**, *154* (6), 1788−1793.
(30) Sajjan, U.; Moreira, J.; Liu, M. Y.; Humar, A.; Chaparro, C.; Forstner, J.; Keshavjee, S. A Novel Model to Study Bacterial Adherence to the Transplanted Airway: Inhibition of Burkholderia Cepacia Adherence to Human Airway by Dextran and Xylitol. *J. Heart Lung Transpl* **2004**, *23* (12), 1382−1391.
(31) Wulandari, P.; Nagahiro, T.; Fukada, N.; Kimura, Y.; Niwano, M.; Tamada, K. Characterization of Citrates on Gold and Silver Nanoparticles. *J. Colloid Interface Sci.* **2015**, *438*, 244−248.
(32) Borodko, Y.; Habas, S. E.; Koebel, M.; Yang, P. D.; Frei, H.; Somorjai, G. A. Probing the Interaction of Poly(vinylpyrrolidone) with Platinum Nanocrystals by UV-Raman and FTIR. *J. Phys. Chem. B* **2006**, *110* (46), 23052−23059.
(33) Huang, C. C.; Chen, C. T.; Shiang, Y. C.; Lin, Z. H.; Chang, H. T. Synthesis of Fluorescent Carbohydrate-Protected Au Nanodots for Detection of Concanavalin A and Escherichia coli. *Anal. Chem.* **2009**, *81* (3), 875−882.
(34) Loynachan, C. N.; Soleimany, A. P.; Dudani, J. S.; Lin, Y. Y.; Najer, A.; Bekdemir, A.; Chen, Q.; Bhatia, S. N.; Stevens, M. M. Renal Clearable Catalytic Gold Nanoclusters for in vivo Disease Monitoring. *Nat. Nanotechnol* **2019**, *14* (9), 883−890.
(35) Lin, A. Q.; Liu, Q. Y.; Zhang, Y. H.; Wang, Q.; Li, S. R.; Zhu, B. J.; Miao, L. Y.; Du, Y.; Zhao, S.; Wei, H. A Dopamine-Enabled Universal Assay for Catalase and Catalase-Like Nanozymes. *Anal. Chem.* **2022**, *94* (30), 10636−10642.
(36) Wang, Z. Z.; Shen, X. M.; Gao, X. F.; Zhao, Y. L. Simultaneous Enzyme Mimicking and Chemical Reduction Mechanisms for Nanoceria as a Bio-antioxidant: a Catalytic Model Bridging Computations and Experiments for Nanozymes. *Nanoscale* **2019**, *11* (28), 13289−13299.
(37) Brzuszkiewicz, E.; Bruggemann, H.; Liesegang, H.; Emmerth, M.; Olschlager, T.; Nagy, G.; Albermann, K.; Wagner, C.; Buchrieser, C.; Emody, L.; et al. How to Become a Uropathogen: Comparative Genomic Analysis of Extraintestinal Pathogenic Escherichia coli Strains. *Proc. Natl. Acad. Sci. U. S. A.* **2006**, *103* (34), 12879−12884.
(38) Schembri, M. A.; Klemm, P. Biofilm Formation in a Hydrodynamic Environment by Novel FimH Variants and Ramifications for Virulence. *Infect. Immun.* **2001**, *69* (3), 1322−1328.
(39) D'Amico, G.; Bazzi, C. Pathophysiology of Proteinuria. *Kidney Int.* **2003**, *63* (3), 809−825.
(40) Hung, C. S.; Dodson, K. W.; Hultgren, S. J. A Murine Model of Urinary Tract Infection. *Nat. Protoc* **2009**, *4* (8), 1230−1243.
(41) Worby, C. J.; Schreiber, H. L.; Straub, T. J.; van Dijk, L. R.; Bronson, R. A.; Olson, B. S.; Pinkner, J. S.; Obernuefemann, C. L. P.; Munoz, V. L.; Paharik, A. E.; et al. Longitudinal Multi-omics Analyses Link Gut Microbiome Dysbiosis with Recurrent Urinary Tract Infections in Women. *Nat. Microbiol* **2022**, *7* (5), 630−639.
(42) Siddiq, D. M.; Darouiche, R. O. New Strategies to Prevent Catheter-associated Urinary Tract Infections. *Nat. Rev. Urol* **2012**, *9* (6), 305−314.
(43) Guiton, P. S.; Hannan, T. J.; Ford, B.; Caparon, M. G.; Hultgren, S. J. Enterococcus faecalis Overcomes Foreign Body-Mediated Inflammation To Establish Urinary Tract Infections. *Infect. Immun.* **2013**, *81* (1), 329−339.
(44) Guiton, P. S.; Hung, C. S.; Hancock, L. E.; Caparon, M. G.; Hultgren, S. J. Enterococcal Biofilm Formation and Virulence in an Optimized Murine Model of Foreign Body-Associated Urinary Tract Infections. *Infect. Immun.* **2010**, *78* (10), 4166−4175.
(45) Zhang, D. Y.; Liu, H. K.; Li, C. Y.; Younis, M. R.; Lei, S.; Yang, C.; Lin, J.; Li, Z. M.; Huang, P. Ceria Nanozymes with Preferential Renal Uptake for Acute Kidney Injury Alleviation. *ACS Appl. Mater. Interfaces* **2020**, *12* (51), 56830−56838.
(46) Si, R.; Zhang, Y. W.; You, L. P.; Yan, C. H. Self-organized Monolayer of Nanosized Ceria Colloids Stabilized by Poly-(vinylpyrrolidone). *J. Phys. Chem. B* **2006**, *110* (12), 5994−6000.
(47) Alpaslan, E.; Geilich, B. M.; Yazici, H.; Webster, T. J. pH-Controlled Cerium Oxide Nanoparticle Inhibition of Both Gram-Positive and Gram-Negative Bacteria Growth. *Sci. Rep.* **2017**, *7*, 45859.
(48) Jang, H.; Lee, C.; Hwang, Y.; Lee, S. J. Concanavalin A: coordination diversity to xenobiotic metal ions and biological consequences. *Dalton Trans* **2021**, *50* (48), 17817−17831.
(49) Edelman, G. M.; Cunningham, B. A.; Reeke, G. N.; Becker, J. W.; Waxdal, M. J.; Wang, J. L. The covalent and three-dimensional structure of Concanavalin A. *Proc. Natl. Acad. Sci. U.S.A.* **1972**, *69* (9), 2580−2584.
(50) Larrosa, M.; Truchado, P.; Espin, J. C.; Tomas-Barberan, F. A.; Allende, A.; Garcia-Conesa, M. T. Evaluation of Pseudomonas Aeruginosa (PAO1) Adhesion to Human Alveolar Epithelial Cells A549 Using SYTO 9 Dye. *Mol. Cell Probe* **2012**, *26* (3), 121−126.

https://doi.org/10.1021/acsnano.3c12783
ACS Nano XXXX, XXX, XXX−XXX